

Spatial Distribution of the Speed of Sound in Biological Materials with the Scanning Laser Acoustic Microscope

PAUL M. EMBREE, STUDENT MEMBER, IEEE, KALERVO M. U. TERVOLA, STEVEN G. FOSTER, AND WILLIAM D. O'BRIEN, JR., SENIOR MEMBER, IEEE

Abstract—An important ultrasonic propagation property for tissue characterization is the speed of sound. The scanning laser acoustic microscope (SLAM) provides the capacity to determine the speed of sound in tissue specimens or portions of specimens on the submillimeter scale. This capability potentially can be utilized to develop indices that quantify the spatial gradient of the tissue's speed of sound. An automated technique for determining the speed of sound using the SLAM has been developed. It is now possible to study quantitatively the degree of tissue heterogeneity from SLAM measurements of the speed of sound distribution.

I. INTRODUCTION

THE FUNDAMENTAL examination of biological tissue with ultrasound can lead to important diagnostic capabilities. In order to quantify tissue characteristics with ultrasound, the ultrasonic propagation properties of normal and pathological tissues must be characterized and cataloged. The ultrasonic propagation properties of tissues, namely, attenuation, absorption, and speed, are determined largely at the macromolecular level. This idea is supported by studies in blood dating back over thirty years ago [1]. A qualitative relationship appears to exist between ultrasonic propagation properties and tissue constituents [2], [3]. Quantitative relationships have also been observed between the ultrasonic propagation properties (usually in the low-MHz frequency range) and the tissue's water, protein, and collagen concentrations [4]. Thus, an important ultrasonic propagation property is the speed of sound for characterizing tissue [2]–[7]. Since tissue appears not to be greatly dispersive, the measurement of the speed of sound at 100 MHz provides a reasonable estimate of the speed of sound at lower frequencies, which are used in clinical applications. At 100 MHz greater spatial information can be derived, thus providing a quantitative measure of the speed gradient, a quantity that affects ultra-

sonic scattering. In this work a technique is described that determines the speed of sound and its spatial variation in tissue using the scanning laser acoustic microscope (SLAM) [8], [9]. A companion paper describes a technique for the determination of the ultrasonic attenuation coefficient measurement with the SLAM [10].

The details of operation of the SLAM (Sonomicroscope 100®) have been described elsewhere [11]–[15]. Briefly, a laser scans the lower surface of the mirror-like coverslip in order to detect mechanical disturbances induced by the 100 MHz ultrasonic energy which has passed through the specimen from below. The SLAM provides three different television type images as shown in Fig. 1. The optical (laser scan) transmission image (Fig. 1(a)) allows the operator to position the sample in the center of the 3 mm (horizontal) by 2 mm (vertical) field of view. The acoustic image (Fig. 1(b)) is an indication as to the amount of ultrasonic energy that has passed through the sample. This signal is proportional to the envelope of the laser detector output. In this image dark areas correspond to areas of high ultrasonic attenuation and light areas to areas of low attenuation. The interference image (Fig. 1(c)) is produced by electronically mixing the laser detector output with a 100-MHz reference signal.

The interference image consists of approximately 39 light and dark vertical bands that represent locations of constant phase contours of the ultrasonic wave after it has traversed through the specimen. These bands are called interference lines. In the homogeneous saline solution (the normal coupling medium for tissue samples) the vertical interference lines should be straight and equally spaced. When a slice of tissue (usually 300 to 900 μm thick) is placed in the saline solution, the interference lines shift to the right as they pass from the saline into the tissue, indicating that the tissue has a higher speed of sound than that of the saline. In an area of tissue where the thickness is constant, the interference lines appear somewhat corrugated; that is, they do not appear as straight as those from the homogeneous coupling medium. A portion of this variation is due to electrical and mechanical noise in the SLAM and can be reduced by signal processing. The re-

Manuscript received April 1984; revised September 1984. This work was supported in part by the National Institute of Health under contract CA 36029 and AM 21557.

P. M. Embree and W. D. O'Brien, Jr., are with the Bioacoustics Research Laboratory, Department of Electrical and Computer Engineering, University of Illinois, 1406 W. Green St., Urbana, IL 61801, USA.

K. M. U. Tervola is with the University of Oulu, Department of Electrical Engineering, SF 90570 Oulu 57, Finland.

S. G. Foster is with Therm-X, Inc., 701 Devonshire, Bldg. Bl #10, Champaign, IL 61820, USA.

®Registered trademark of Sonoscan, Inc.

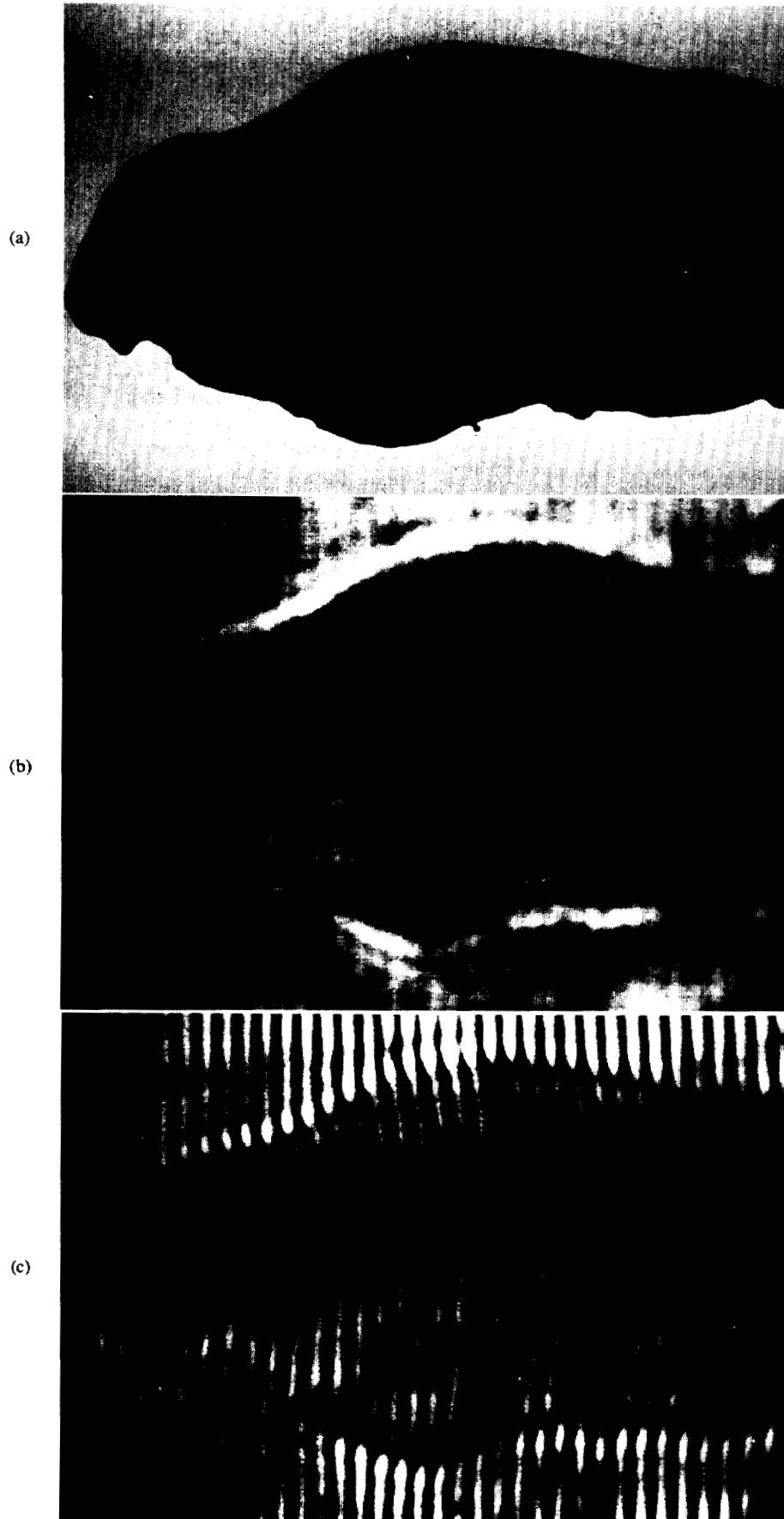


Fig. 1. Photographs from the SLAM monitors of a 550- μm -thick rat liver specimen. (a) Optical image. (b) Acoustic image. (c) Interference image.

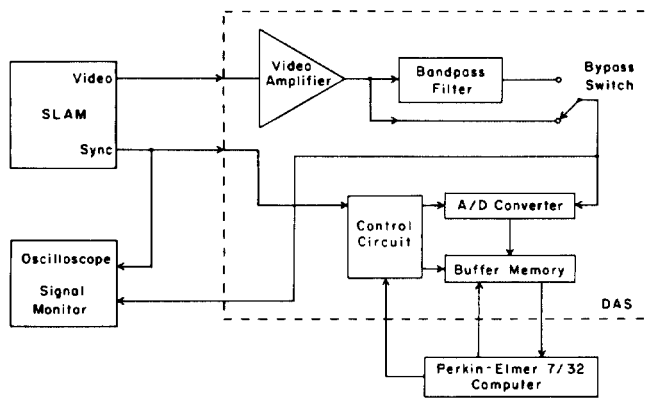


Fig. 2. Block diagram of data acquisition system used to digitize the SLAM images.

maining variation is thought to be due to changes in the microscopic speed of sound. The emphasis of the paper is to describe the procedures by which speed and its gradient are measured. To do this the interference lines are subjected to an automated analysis technique which is described herein. Also, an analysis of the uncertainty in the measurement will be discussed.

II. DATA ACQUISITION SYSTEM

The interference image produced by the SLAM is digitized by a data acquisition system (DAS) that was specifically designed and fabricated for this application (Fig. 2) [9]. The principal design consideration was to provide the capability to digitize the images from the SLAM without requiring any modifications to the microscope. To do this the data acquisition system utilizes the composite video signal and sync signals generated by the SLAM. The DAS consists of a video amplifier, a bandpass filter, an analog-digital (A/D) converter and a high-speed buffer memory, all of which interfaces the SLAM to the Perkin-Elmer 7/32 32-bit minicomputer. The amplified video signal is monitored on an oscilloscope by the microscope operator to assure that the signal is using the full dynamic range of the A/D converter.

The interference image consists of about 39 vertical interference lines that are approximately spaced equally across the image. In this mode the video signal is relatively narrow-band for purposes of extracting the interference images. The duration of the video portion of a horizontal raster line is $52.5 \mu\text{s}$, and the average time between signal peaks is $1.35 \mu\text{s}$ for an average frequency of 740 kHz. Thus, the signal-to-noise (S/N) ratio of the interference image can be improved significantly by the addition of a bandpass filter. A sixth-order Chebyshev filter was designed for this purpose. The bandpass of this filter is between 700 and 900 kHz with a ± 0.5 dB ripple. The addition of the filter has allowed for the speed of sound to be measured in quite highly attenuating specimens for which the interference lines might not normally be well defined. The effect of this bandpass filter on the speed of sound measurement is difficult to determine analytically. However, experimental evidence, to be described later, has

confirmed that there is a negligible change in the speed measurement due to the bandpass filter.

An interference image consists of 482 horizontal raster lines. To digitize the image, one raster line at a time is digitized at 28.6 MHz and stored in the buffer memory. The 8-bit, 30 MHz A/D converter is a TRW 1007PCB. Approximately 1514 data points per raster line are digitized. The buffer memory can store 2048 samples in a circular fashion. The memory is arranged as 1024×16 bits of fast bipolar RAM (random access memory) (access time of 35 ns); each of the 1024 halfwords consists of two samples. This arrangement of samples effectively halves the access time, thus allowing the memory to operate predictably at 30 MHz. The data of one raster line are then transferred into the mini-computer memory at a rate of about 50 kHz. This operation is repeated for all 482 lines. Thus, the completely digitized interference image consists of 729 748 picture elements.

III. ENHANCEMENT OF THE INTERFERENCE IMAGE

Several programs were developed to enhance the interference image. These programs have three objectives:

- 1) to minimize the effect of the horizontal jitter which the interferogram image experiences;
- 2) to improve the S/N ratio of the image; and
- 3) to define precisely the position of the equal phase fronts.

A line printer output of a typical saline solution interferogram image is shown in Fig. 3. A program has digitized the video signal, averaged it eight times (the number of averages is selectable between 1 and 64), and stored the data on magnetic tape for subsequent processing. In this case the data were subjected to a histogram equalization routine in order to improve its contrast for the line printer (Printronix model 300). Fig. 3 provides an image record of the interferogram image without the need to develop photographic film.

An algorithm was developed to compensate for the slight and somewhat periodic horizontal jitter of the interference image by averaging it out. The horizontal image jitter from the SLAM is illustrated in Fig. 4. The three interference lines shown in the figure were obtained from three different interferogram images of water that were digitized in several different ways. In each case a correlated receiver algorithm (to be discussed below) was applied to the digitized waveform to yield the relative position of the interference line. Ideally, the interference lines should be straight because the medium is homogeneous. The interference line shown in Fig. 4(a) was obtained by averaging *each* raster line 64 times, correlating the result and then proceeding to the next adjacent raster line. The perturbation of the horizontal jitter is about ± 2 samples (± 70 ns). This represents a ± 5 percent error in the average distance between interference lines and would result in a ± 0.2 percent error in the speed of sound. The jitter exhibits a periodic component of about five raster lines per cycle; hence, the perturbation has a period of

SALINE FILTER 370 FEB18
AVERAGE = 8

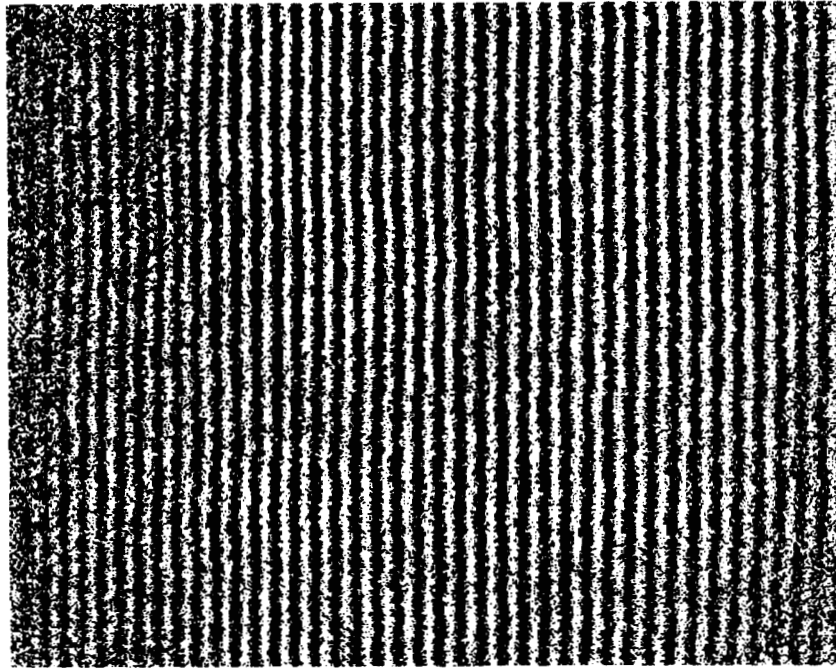


Fig. 3. Enhanced interference image of a blank field in which the medium was water; that is, no biological tissue specimen was present. The image data were averaged eight times. The image is a histogram equalized to improve its contrast for the line printer.

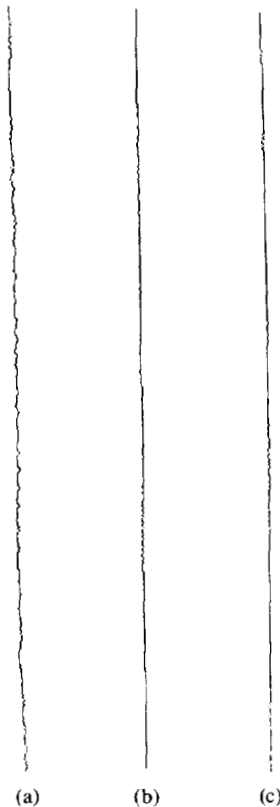


Fig. 4 Separate interference lines from three different interferogram images which demonstrate the horizontal jitter to various degrees through three different averaging schemes. (a) Each raster line was independently averaged 64 times. (b) Blocks of 60 raster lines were block averaged 64 times. (c) Running average of 64 times.

about 10 s, which would not be visually perceptible. However, its minimization or elimination would decrease the potential uncertainty in determining the speed of sound. Thus, two other averaging schemes have been investigated. Fig. 4(b) shows an interference line which was divided into eight blocks of 60 raster lines each. Each block was averaged as a whole; that is, all the lines in the block were digitized and averaged at once instead of only a single line at a time. This method appears to eliminate the jitter within a block but jitter is still apparent between consecutive blocks. Though it would be desirable to store the entire interferogram image in memory and provide for frame averaging, this would require 1.5 megabytes of memory and exceed the present computer system capacity. For these reasons a sliding block averaging program was developed, where a running average was performed on a block-by-block basis. This result is shown in Fig. 4(c), and the algorithm is shown in the flowchart of Fig. 5.

The number of raster lines in the block is equal to the number of averages requested. The block of raster lines is arranged in order of position in the image. The top raster line of the block is averaged $n - 1$ times, the next raster line is averaged $n - 2$ times, and so on, until the next to the last line in the block is averaged once. The program then digitizes each line once more, adding these to the previous lines. The top line is now averaged n times and is transferred to magnetic tape. The entire block moves down one raster line and the averaging process continues until all 482 raster lines have been stored on magnetic tape. Fig. 4(c) shows the result of this program

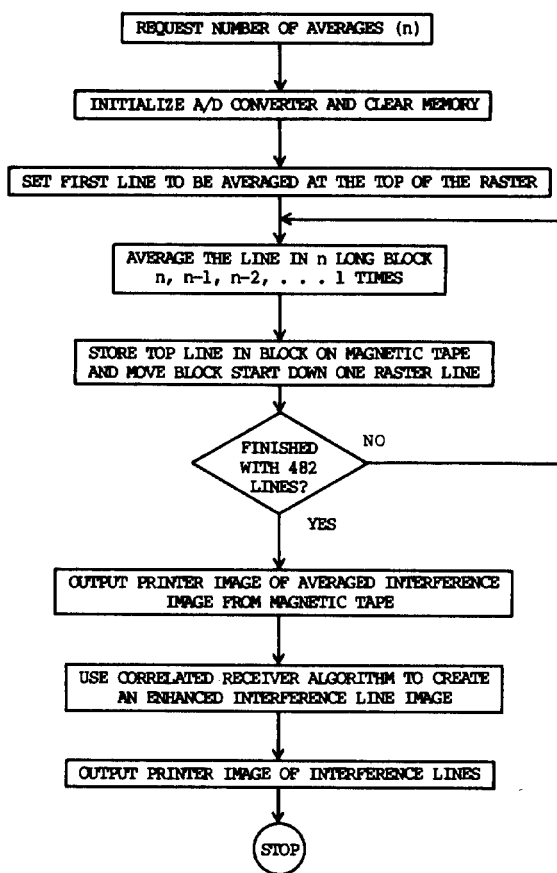


Fig. 5. Flowchart of programs to digitize and enhance the interference image.

for one interference line. When compared to the other two lines, the periodic jitter appears to have been eliminated, thus leaving only a random system noise jitter.

Once the interference image has been averaged the required number of times, it is then enhanced with the correlated receiver algorithm. This program compares the waveform on each raster line to that of a replica of an ideal cross section of an interference line that is stored in memory; detects where relative maxima occur in the correlated result; and defines the positions of the interference lines on the raster line. The length of the stored replica was investigated. The S/N ratio improves as the length increases but the program's execution time increases likewise. A correlation length of 17 was chosen because this is about half of the average period, and this gave sufficient interference line definition without excessive computation time. The shape of the reference waveform was obtained experimentally by averaging one raster line of a saline solution image for a long time.

Applying the correlator receiver algorithm to a single, averaged raster line yields approximately 39 data points, each of which represent the center of 39 interference lines at that particular raster line location. Thus the enhanced interference image consists of interference lines that are each one data point in width. Fig. 6 shows the results of this program on the same image shown in Fig. 3. An important characteristic of this image is that it is represented by a more manageable 482×39 element array.

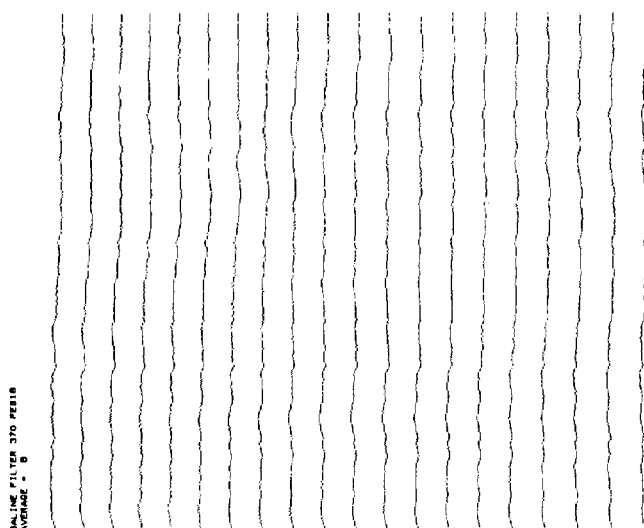


Fig. 6. Interference line image of water which has been enhanced by a correlator receiver technique (same image data as Fig. 3).

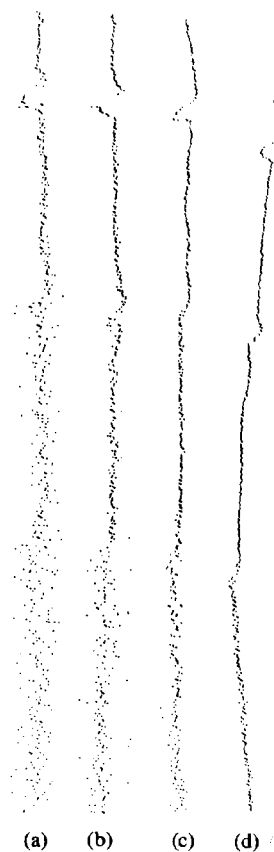


Fig. 7. Interference lines showing the improvement with averaging. (a) 1 average. (b) Four averages. (c) 16 averages. (d) 64 averages.

By increasing the number of averages, the noise in the image is reduced, and the quality of the resulting interference lines is improved. Fig. 7 illustrates this improvement on one interference line which was averaged once, four, 16, and 64 times. Typically, a doubling of the number of averages results in a 3-dB increase in the signal to noise ratio. Thus, the interference line shown in Fig. 7(d) resulted from an averaged image with 18 dB less noise than Fig. 7(a).

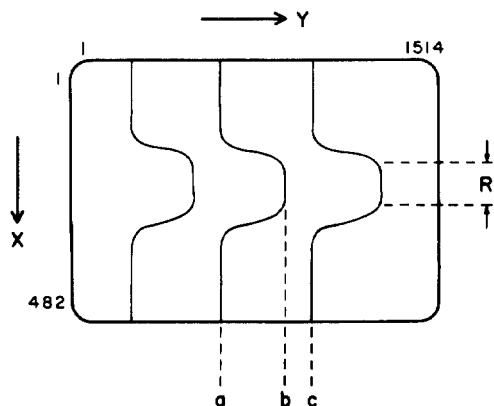


Fig. 8. Schematic representation of the fringe shift $N = ab/ac$.

IV. CALCULATION AND STATISTICS OF THE SPEED OF SOUND

The calculation of the specimen's speed of sound c_x from the interference line image can be performed by using (derived in [5])

$$c_x = \frac{c_0}{\sin \theta_0} \sin \left\{ \tan^{-1} \left[\frac{1}{(1/\tan \theta_0) - (N\lambda_0/T \sin \theta_0)} \right] \right\} \quad (1)$$

where c_0 is the speed of sound in the reference medium; λ_0 is the wavelength of sound in that same medium; θ_0 is the angle of the beam from the normal in the reference medium; T is the thickness of the specimen; and N is the normalized lateral interference line shift ($N = ab/ac$ —see Fig. 8). Using Snell's law, θ_0 can be determined for the reference medium by

$$\theta_0 = \sin^{-1} \left[\frac{c_0}{c_s} \sin \theta_s \right] \quad (2)$$

where c_s is the speed of sound in the fused-silica stage (5968 m/s), and $\theta_s = 45^\circ$ is the angle at which the generated sound waves travel through the stage with respect to the normal. In this project the materials being examined are generally biological specimens, where normal saline solution (0.9 percent NaCl) is the common reference medium. Saline has a known speed of 1507 m/s at a temperature of 22°C [16], hence $\theta_0 = 10.29^\circ$. The speed of sound in saline increases by about 4 m/s for each degree rise in temperature [16]. The ambient temperature was controlled with $\pm 1^\circ\text{C}$ giving a possible ± 0.3 percent error in the speed of sound of the reference media.

The previous method employed [5], [6] to determine the speed of sound in a specimen was performed manually by assessing the location of lines a , b , and c (see Fig. 8) and the distances ab and ac from either photographs of the TV monitor or directly from the monitor in order to calculate the normalized lateral fringe shift $N = ab/ac$. For this particular method the operator had to determine the best fit of the fringe lines and choose points from which to measure the distances ab and ac . This procedure

was quite time-consuming and provided, in general, only one velocity value per interference line and only a few velocity values for the specimen. The computer program described here automates the measurement process, increases the area of tissue from which the speed of sound can be calculated, and involves minimal operator interaction.

As can be seen from the enhanced interference image (Fig. 6), the interference lines are not always continuous. They can also have a significant amount of jitter due to system noise. In order to automate the speed of sound determination, it is necessary for an algorithm first to identify the discrete interference lines. A computer program was written to follow the interference lines, fill in the missing data points, and smooth them by curve-fitting. The start of each interference line is determined by counting the interference line positions of the first ten raster lines. Any positions included in more than three of the ten possible raster lines (the interference line is assumed to be somewhat straight and vertical) become the starting place for the identified line. The line identification now proceeds from the first raster line to the last. If a line is not continuous (i.e., a point is not within ± 20 samples of the previous raster line position) then the program adds a point at a position determined by a linear interpolation based on the nearest ten points. The program informs the user how many points have been added in which line (interference lines are numbered sequentially from left to right). The resulting continuous interference lines are then smoothed by a sliding 17-point quadratic curve-fitting algorithm, which can be considered a low-pass filtering operation.

Two adjacent interference lines are used to determine the distance ac . In order to do so, the specimen must be placed on the microscope stage in such a way that the specimen's boundaries are within the horizontal boundaries, which are defined by $x = 51$ to 432 (Fig. 8). The top ($x = 1$ to 50) and bottom ($x = 433$ to 482) 50 points each (100 points total) of each pair of interference lines are used to determine the location of lines a and c . The best-fitting straight lines for a and c are found by using a least-squares linear curve fit. If lines a and c are perfectly vertical in orientation, the slope of these lines will be zero. The y intercept of these lines will vary from 0 to 1513, depending upon the location of the interference lines. After the equations for lines a and c are defined, the distance ac is calculated for each point $x = 1$ to 50 and $x = 433$ to 482 , and this average value for ac is used as the denominator for determining the normalized lateral fringe shift for the interference line within region R .

The width of region R (see Fig. 8), where the distance ab is calculated, is a variable under operator control. The value of R can range from one up to 382, the latter being the maximum extent, since the top and bottom 50 data points each are utilized for the calculation of ac . The rationale for this variable region is that not all of the data in the region between raster lines 51 and 432 may be useful for the following reasons.

- 1) The specimen may not occupy the entire region between raster lines 51 and 432.
- 2) The specimen may not be uniformly thick over this region because of edge effects.
- 3) It may be necessary to avoid certain inhomogeneities in the tissues, such as blood vessels. All of these can be assessed by the acoustic microscopist from the images. The horizontal distance ab is calculated R times, and N is determined using each of these ab values and the average ac value previously calculated for that area of the specimen. Given the sample thickness, the speed of sound data set (R total values) is determined from (1).

Various statistical parameters are calculated from each speed of sound data set; namely, the standard deviation, mean, mode, median, skewness, and kurtosis.

The standard deviation is defined as [17]

$$S = \sqrt{\frac{1}{R} \sum_{j=1}^R (x_j - \bar{x})^2} \quad (3)$$

where \bar{x} is the mean value; R is the number of samples; and x_j is the j th speed value along the region R . The standard deviation is a measure of the concentration of values around the mean.

The mode is that value which occurs more frequently than any other value; graphically it appears as the peak of a distribution. Of a set of numbers arranged in order of magnitude, the median is the value of the exact middle position of the set. In this program, to calculate the median the data set length is always chosen to be odd, thus requiring only one algorithm.

Skewness is an indication of the "sidedness" of a distribution with respect to its mean. By definition [17]

$$\text{skew} = \frac{3(\bar{x} - \text{median})}{S}. \quad (4)$$

The distribution is said to be skewed right, and skew will be positive if more values of the data set are to the right of the mean. Similarly if skew is negative the distribution is skewed left.

Kurtosis is a measure of the shape of distribution which reveals the degree of peakedness of the distribution as compared to a normal distribution. Kurtosis is defined using a dimensionless fourth moment around the mean [17] or

$$\text{kurtosis} = \frac{\frac{1}{R} \sum_{j=1}^R (x_j - \bar{x})^4}{S^4} - 3. \quad (5)$$

For a normal (Gaussian) distribution kurtosis would be zero. A distribution is said to be leptokurtic (spiky, very peaked) if kurtosis is greater than zero and platykurtic (flat) if less than zero [17].

V. DISCUSSION OF MEASUREMENT UNCERTAINTIES

The effect of the bandpass filter (described earlier) and the line-following program on two representative inter-

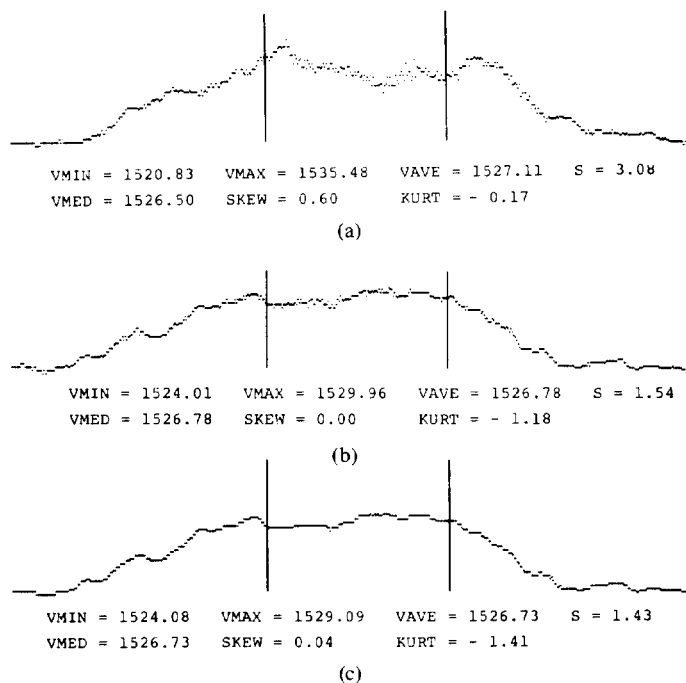


Fig. 9. Fringe shift curves and statistical speed-of-sound values for two lines of a 740- μ m-thick rat liver sample. (a) No filter and no line following program. (b) Filter only. (c) Filter and line following program.

ference lines taken from an image of a 740- μ m-thick liver sample is shown in Fig. 9. Fig. 9(a) shows the normalized fringe shift curve resulting from unfiltered, unsmoothed lines that were averaged eight times. All averaging of the interferogram images was performed with the running average routine. Fig. 9(b) shows the fringe shift curve resulting from the same lines with filtering. Fig. 9(c) shows the resultant fringe shift curve with filtering and the line-following program. All three interferogram lines yielded the same mean speed of sound value (1527 m/s). There was a trend of decreasing standard deviation with increasing processing of the interferogram. A comparison of these numerical values tend to indicate that the effect of filtering and line smoothing has a negligible influence upon the mean value and tends to improve the measurement technique by reducing the standard deviation.

As (1) shows, the measurement of the speed of sound is dependent on two quantities which are subject to experimental error; that is, the normalized fringe shift N and the specimen thickness T . (The measurement temperature is assumed to stay constant.) The remaining variables are well-known constants or physical dimensions that will not change with each experiment. Fig. 10 graphically illustrates the error in the speed of sound measurement in a specimen with a speed of sound of 1545 m/s as T and N are changed by a small percentage from 370 μ m and 0.61, respectively. This type of parametric graph can be used by the operator to determine the approximate error of a particular measurement due to variations in thickness. For example, if the error in T is -12 percent and the error in N is +12 percent, the resulting error in speed is 10 m/s or 0.65 percent of the 1545 m/s nominal value.

The standard deviation of the system was measured ex-

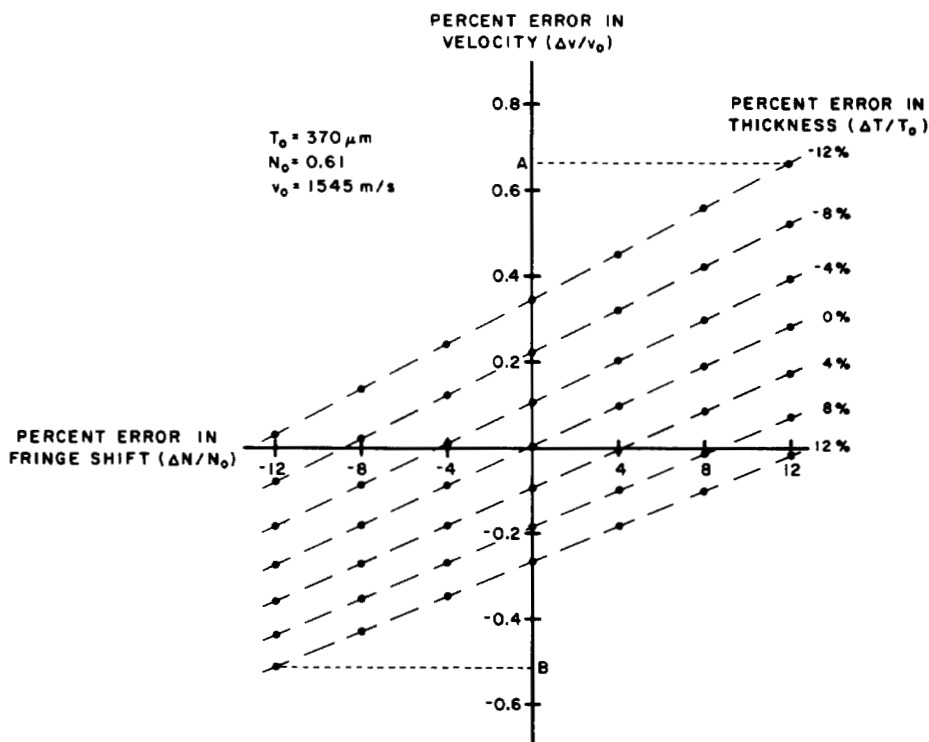


Fig. 10. Percent error in velocity versus percent error in fringe shift and percent error in thickness in a specimen having a velocity of 1545 m/s. Point A represents a +10 m/s error (0.66 percent of 1545 m/s). Point B represent a -8 m/s error (0.51 percent of 1545 m/s).

perimentally using a 370- μm layer of saline as a specimen. This was done because saline, the reference media, can be considered an ideal homogeneous specimen, so the measurement errors are due to the microscope and data acquisition system. The first measurement was performed using the filter and the second without filter. The range R included 128 points. The experiments yielded values of 2 and 3 m/s for the standard deviation, respectively. The precision of the system was in the range from -0.2 percent to +0.4 percent in both cases.

The accuracy of this technique was determined by using a drop of Dow Corning 710 oil (150 μm thick, eight averages using the running average algorithm), which does not mix with saline. The measurement result was 1405 m/s, which can be compared to the published value of 1378 m/s [18] for a difference of +1.9 percent. This could be due to dispersion. The standard deviation of the velocity distribution was 1.9 m/s, about 0.1 percent of the mean value.

VI. ILLUSTRATION OF THE TECHNIQUE

The following experiment was conducted to illustrate the technique. A white ICR female mouse approximately six to seven months old was sacrificed by means of cervical dislocation so as to not introduce any drugs into the tissues. The liver was quickly excised (within 5 min post-mortem) and immediately placed in an isotonic saline solution. The sample was trimmed with a razor blade into a rectangular piece suitable for viewing with the SLAM. The speed of sound can only be determined by this tech-

```

NUMBER OF AVERAGES = 4
THICKNESS (M) = 0.00046
LINE#   SLOPE   YBAR
  22    -0.02   798.88
LINE#   SLOPE   YBAR
  23    -0.02   838.32
NS = 210  NE = 270  N = 61
AVERAGE FN = 1.19533
NMAX = 1.26496  NMIN = 1.08027
VMIN (M/S) = 1561.348  MVAX (M/S) = 1571.029
AVERAGE SPEED (M/S) = 1567.367
STANDARD DEVIATION (M/S) = 2.313
PLAYKURTIC -0.55
MEDIAN SPEED (M/S) = 1566.490
SKEWED RIGHT 1.137
MODE OCCURS AT 1566M/S  VALUE OF 23.00

```

Fig. 11. Typical output of the program that calculates the speed-of-sound statistical data for one pair of interference lines. (Data for lines 22 and 23 are shown).

nique if there is no discontinuity of the interference line between the saline and tissue. Thus, the edges of the specimen are bevelled.

The sample was positioned on the plastic sheet in the center of the microscope slide, and it was surrounded by a spacer of known thickness slightly smaller than the sample. This way the specimen thickness is the same as that of the spacer, and the spacer prevents the sample from being crushed or distorted by the coverslip. The area surrounding the tissue is filled with saline, which serves as the known reference medium.

The typical output data of a program that calculates all of the previously described speed of sound statistical data are shown in Fig. 11 for a 460- μm -thick fresh mouse liver specimen that was running-block averaged four times. The output is shown for the 22nd and 23rd interference lines.

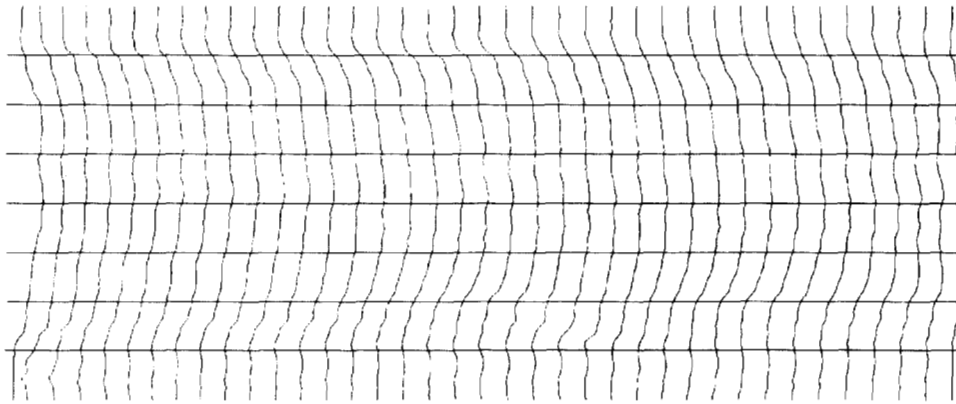


Fig. 12. Smoothed interference lines after running line fitting program for 917- μ m-thick rat liver sample. The horizontal lines in the output are placed every 60 raster lines to simplify the location of region R.

TABLE I
STATISTICAL SPEED OF SOUND DATA FOR 917 μ m THICK LIVER SAMPLE
AVERAGED OVER 128 POINTS HORIZONTALLY. THIRTY-ONE POINTS ACROSS
THE SAMPLE ARE SHOWN.

LINE #	NS	NE	SLOPE1	YBAR1	SLOPE2	YBAR2	AVE N	N MIN	N MAX	VMIN	VMAX	VAVE	SIGMA	KURTOSIS	VMED	SKEM
8	170	297	-0.02	262.9	-0.02	297.6	1.0398	0.8920	1.1343	1529.05	1535.66	1532.77	1.65	-0.98	1532.35	0.7
9	170	297	-0.02	297.6	-0.02	332.2	1.0452	0.8750	1.1685	1528.63	1536.02	1532.91	1.95	-0.74	1532.52	0.6
10	170	297	-0.02	332.2	-0.02	367.1	1.0490	0.9072	1.1681	1529.44	1535.91	1533.00	1.75	-0.82	1532.37	0.7
11	170	297	-0.02	367.1	-0.02	402.2	1.0603	0.9346	1.1882	1530.12	1536.32	1533.29	1.59	-0.60	1532.69	1.1
12	170	297	-0.02	402.2	-0.01	437.6	1.0830	0.9783	1.2032	1531.22	1536.90	1533.86	1.49	-0.51	1533.48	0.7
13	170	297	-0.01	437.6	-0.01	473.2	1.1172	1.0127	1.2428	1532.09	1537.90	1534.72	1.35	-0.74	1534.91	0.4
14	170	297	-0.01	473.2	-0.01	509.2	1.1424	1.0350	1.2692	1532.65	1538.57	1535.36	1.81	-0.90	1534.75	1.0
15	170	297	-0.01	509.2	-0.00	545.9	1.1474	1.0332	1.2612	1532.35	1538.37	1535.49	1.76	-1.02	1535.26	0.3
16	170	297	-0.00	545.9	-0.00	582.1	1.1440	1.0574	1.2437	1533.21	1537.92	1535.40	1.37	-1.09	1534.98	0.8
17	170	297	-0.00	582.1	-0.00	618.7	1.1392	1.0864	1.2344	1533.94	1536.20	1535.78	1.28	-0.74	1535.45	0.7
18	170	297	-0.00	618.7	0.00	655.2	1.1390	1.1010	1.2677	1534.31	1538.53	1536.79	1.19	-1.23	1537.10	-0.7
19	170	297	0.00	655.2	0.00	692.0	1.1297	1.1606	1.2997	1535.62	1539.35	1537.82	1.26	-1.33	1537.98	-0.3
20	170	297	0.00	692.0	0.00	729.4	1.1362	1.1447	1.3263	1535.42	1540.33	1537.74	1.39	-0.98	1538.18	-0.9
21	170	297	0.00	729.4	0.00	766.8	1.1163	1.1177	1.3269	1534.73	1540.04	1537.23	1.42	-0.82	1537.24	-0.0
22	170	297	0.00	766.8	0.00	804.6	1.1024	1.0713	1.3050	1533.56	1539.48	1536.37	1.43	-0.61	1536.65	-0.5
23	170	297	0.00	804.6	0.00	842.4	1.1493	1.0465	1.2289	1532.94	1537.55	1535.53	1.32	-0.48	1535.58	-0.1
24	170	297	0.00	842.4	0.00	880.3	1.1259	1.0163	1.2250	1532.18	1537.32	1534.94	1.28	-0.80	1535.30	-0.8
25	170	297	0.00	880.3	0.00	918.9	1.0968	1.0038	1.2077	1531.86	1537.01	1534.21	1.44	-1.01	1534.47	-0.5
26	170	297	0.00	918.9	-0.00	957.4	1.0625	0.9641	1.1498	1530.86	1535.44	1533.35	1.46	-1.19	1533.48	-0.2
27	170	297	-0.00	957.4	-0.00	995.2	1.0572	0.9661	1.1530	1530.92	1535.63	1533.21	1.43	-0.96	1533.01	0.4
28	170	297	-0.00	995.2	0.00	1032.9	1.0647	0.9757	1.1627	1531.16	1535.87	1533.40	1.27	-0.42	1533.21	0.4
29	170	297	0.00	1032.9	0.00	1070.6	1.0706	0.9854	1.1699	1531.40	1536.05	1533.55	1.15	-0.36	1533.36	0.5
30	170	297	0.00	1070.6	-0.00	1108.4	1.0788	0.9897	1.1471	1531.51	1535.48	1533.75	1.17	-1.04	1534.10	-0.9
31	170	297	-0.00	1108.4	-0.00	1146.2	1.0900	0.9934	1.1794	1531.60	1536.29	1534.04	1.23	-1.31	1534.28	-0.5
32	170	297	-0.00	1146.2	-0.00	1184.2	1.0916	0.9980	1.1544	1531.72	1535.66	1534.07	1.17	-1.08	1534.20	-0.3
33	170	297	-0.00	1184.2	-0.01	1222.4	1.0903	0.9937	1.1714	1531.61	1536.09	1534.04	1.18	-0.44	1534.02	0.0
34	170	297	-0.01	1222.4	-0.01	1260.8	1.0868	0.9879	1.1866	1531.45	1536.53	1533.96	1.37	-1.03	1533.67	0.6
35	170	297	-0.01	1260.8	-0.01	1299.1	1.0746	0.9889	1.1819	1531.49	1536.36	1533.65	1.63	-1.42	1533.23	0.7
36	170	297	-0.01	1299.1	-0.01	1337.1	1.0523	0.9611	1.1616	1530.79	1535.84	1533.09	1.66	-1.42	1532.92	0.2
37	170	297	-0.01	1337.1	-0.00	1375.1	0.9987	0.8866	1.1035	1528.92	1534.38	1531.74	1.63	-1.19	1531.48	0.4
38	170	297	-0.00	1375.1	-0.00	1413.3	0.8916	0.7793	0.9928	1526.23	1531.58	1529.05	1.68	-1.13	1529.02	0.0

AVERAGE VALUES FOR VELOCITY SKEM SIGMA KURTOSIS
1534.3 0.2 1.5 -0.9

The slopes and y intercepts for lines *a* and *c* (see Fig. 8) of these two interference lines are listed. Fig. 11 shows the speed of sound data for interference line 22 between $x = 210$ and $x = 270$ ($R = 61$ data points). The minimum speed (1561.3 m/s), the maximum speed (1571.0 m/s), the average (mean) speed (1567.4 m/s), and the standard deviation (2.3 m/s) are shown. The distribution is playkurtic, skewed to the right of the mean, has a median speed of 1566.5 m/s, and has a mode at 1566 m/s, of which there are 23 values.

The previous illustration indicates the numerical data that can be obtained from a single interference line. By combining many adjacent interference lines into this analysis procedure, a measure of the spatial distribution of the speed of sound within a specimen is provided. Fig. 12 shows the smoothed continuous fringe lines of a 917 μ m rat liver sample. The statistics for each of the 31 line pairs are shown in Table I. For this set of data, the standard deviation is small and the skew and kurtosis values are close to zero, indicating that the liver sample is quite homogeneous. The average speed of sound (1534.3 m/s), av-

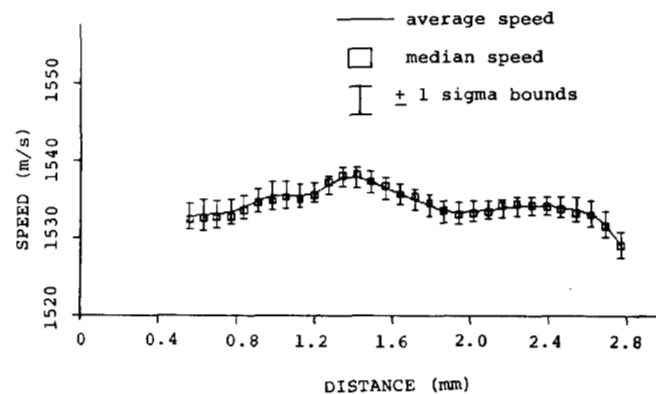


Fig. 13. Speed of sound versus distance across sample.

erage skew (0.2), average standard deviation of the speed of sound (1.5 m/s), and average kurtosis (-0.9) are also shown in Table I. Fig. 13 shows a plot of the average speed of sound; one of the standard deviation error bounds; and the median speed versus distance across the sample. The speed of sound is rather constant, and the standard devia-

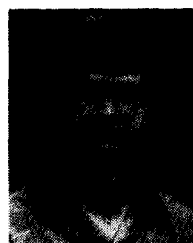
tion is as small as would be expected from a relatively homogeneous specimen.

Using the technique reported herein, the average speed of sound was determined to be 1545 m/s for 28 rat livers [19]. The averaged reproducibility was better than ± 4 m/s, i.e., ± 0.3 percent of the nominal value of 1545 m/s. Even when the results contain the effect of fat on the speed of sound, the values are comparable to those cited in the literature for similar tissues using the SLAM. Frizzell and Gindorf [7] obtained values of 1565 ± 8 m/s for sheep liver and 1567 ± 13 m/s for cat liver. The differences might be due to different fat concentrations, because in [19] it is shown that the speed of sound decreases in a rat liver when the fat concentration increases.

In conclusion, an automated technique for determining the speed of sound at many points across a sample has been developed. The speed of sound data set that is generated is much larger than could be generated manually, thus enabling one to use quantitative statistical parameters to study the degree of tissue specimen heterogeneity.

REFERENCES

- [1] E. L. Carstensen, K. Li, and H. P. Schwan, "Determination of the acoustic properties of blood and its components," *J. Acoust. Soc. Amer.*, vol. 25, pp. 286-289, 1953.
- [2] R. L. Johnston, S. A. Goss, V. Maynard, J. K. Brady, L. A. Frizzell, W. D. O'Brien Jr., and F. Dunn, "Elements of tissue characterization. Part II: ultrasonic propagation properties," in *Proc. Second Int. Symp. on Ultrasonic Tissue Characterization* (National Bureau of Standards Publication 525) M. Linzer, Ed. Washington, DC: U.S. Government Printing Office, 1979.
- [3] F. Dunn, "Ultrasonic attenuation absorption and velocity in tissues and organs," *Proc. First Int. Symp. on Ultrasonic Tissue Characterization* (National Bureau of Standards Publication 453), Washington, DC: U.S. Government Printing Office, 1976, pp. 21-28.
- [4] W. D. O'Brien Jr., "The relationship between collagen and ultrasonic attenuation and velocity in tissue," in *Proc. 1977 Ultrasonics Int.* Guilford, England: IPC Science and Technology, 1977, pp. 194-205.
- [5] S. A. Goss, and W. D. O'Brien Jr., "Direct ultrasonic velocity measurements of mammalian collagen threads," *J. Acoust. Soc. Amer.*, vol. 65, 507-511, 1979.
- [6] W. D. O'Brien Jr., J. Olerud, K. K. Shung, and J. M. Reid, "Quantitative acoustical assessment of wound maturation with acoustic microscopy," *J. Acoust. Soc. Amer.*, vol. 69, 575-579, 1981.
- [7] L. A. Frizzell and J. D. Gindorf, "Measurement of ultrasonic velocity in several biological tissues," *Ultrasound Med. Biol.*, vol. 7, pp. 385-387, 1981.
- [8] P. M. Embree, S. G. Foster, G. Bright, and W. D. O'Brien Jr., "Ultrasonic velocity spatial distribution analysis of biological materials with the scanning laser acoustic microscope," in *Acoustical Imaging*, vol. 13. New York: Plenum, 1983, pp. 203-216.
- [9] S. Foster, "An image digitizing system for a scanning laser acoustic microscope," M.S. Thesis Dept. of Electrical Engineering, University of Illinois, Urbana-Champaign, IL, 1981.
- [10] K. M. U. Tervola, S. G. Foster, and W. D. O'Brien Jr., "Attenuation coefficient measurement technique at 100 MHz with the scanning laser acoustic microscope," *IEEE Trans. Sonics Ultrason.*, vol. SU-32, no. 2, pp. 259-267.
- [11] A. Korpel, L. W. Kessler, and P. R. Palermo, "An acoustic microscope operating at 100 MHz," *Nature*, vol. 323, 110-111, 1971.
- [12] —, "Simultaneous acoustic and optical microscopy of biological specimens," *Nature*, 239, 111-112, 1972.
- [13] —, "Practical high resolution acoustic microscopy," *Acoustical Holography*, G. Wade, Ed. New York: Plenum, 1972, p. 51-71.
- [14] —, "Recent developments with the scanning laser acoustic microscope," in *Acoustical Holography*, P. S. Green, Ed. New York: Plenum, 1974, vol. 5, pp. 15-23.
- [15] L. W. Kessler, "The sonomicroscope," *Proc. 1974 IEEE Ultrason. Symp.*, J. De Klerk, Ed. Cat. No. 74-CHO-896-1 SU. p. 735-737.
- [16] A. D. Pierce, *Acoustics: An Introduction to Its Physical Principles and Applications*. New York: McGraw-Hill, 1981.
- [17] J. L. Bruning and B. L. Kintz. *Computational Handbook of Statistics*. Glenview, IL: Scott, Foresman and Company, 1968.
- [18] F. Dunn, P. D. Edmonds, and W. J. Fry, "Absorption and dispersion of ultrasound in biological media," in *Biological Engineering*, H. P. Schwan, Ed. New York: McGraw-Hill, 1969, p. 205.
- [19] K. M. U. Tervola, M. A. Grummer, A. M. Mravca, J. W. Erdman, and W. D. O'Brien Jr., "Ultrasonic attenuation and velocity properties in rat liver as a function of fat content—Study at 100 MHz using a scanning laser acoustic microscope," *J. Acoust. Soc. Am.*, to be published.



Paul M. Embree (S'80) was born in Reading, PA, on September 27, 1959. He received the B.S. degree in electrical engineering from Lehigh University, Bethlehem, PA, in 1981 and the M.S. degree in electrical engineering from the University of Illinois, Urbana, IL, in 1982.

From 1981 to 1983 he worked for AT&T Bell Laboratories as a Member of the Technical Staff. Currently he holds the position of Research Assistant at the Bioacoustics Research Laboratory at the University of Illinois. In his current research he is

investigating signal processing approaches to accurate ultrasonic measurement of blood flow.

Kalervo M. U. Tervola, for a photograph and biography see page 265 of the March 1985 issue of this TRANSACTIONS.

Steven G. Foster, photograph and biography not available at the time of publication.

William D. O'Brien, Jr., for a photograph and biography please see page 25 of the January 1985 issue of this TRANSACTIONS.